Feed-out of Rear Surface Perturbation due to Rarefaction Wave in Laser-Irradiated Targets

K. Shigemori, M. Nakai, H. Azechi, K. Nishihara, R. Ishizaki,* T. Nagaya, H. Nagatomo, and K. Mima
Institute of Laser Engineering, Osaka University 2-6 Yamada-Oka, Suita, Osaka, 565-0871 Japan
(Received 18 February 2000)

We report experimental results on hydrodynamic perturbation transfer from the rear to the front of laser-irradiated targets. Flat polystyrene foils with rear-surface perturbations were irradiated by partially coherent light. We observed phase inversion of the rear surface after the shock breakout at the rear surface. Perturbations on the laser-irradiated surface arose due to the rippled rarefaction wave. Experimental results were well reproduced by a simple model with unperturbed hydrodynamic quantities calculated from the one-dimensional simulation.

PACS numbers: 52.50.Jm, 52.35.Py, 52.70.La

Hydrodynamic instabilities are crucial for the inertial confinement fusion (ICF) target design because they limit the achievable fusion performance. In the laser-irradiated target, initial target roughness on the laser-irradiated surface is a direct trigger of the hydrodynamic instabilities such as the Rayleigh-Taylor (RT) instability [1]. Likewise, intensity nonuniformity of irradiation laser also gives a perturbation on the target as "imprint" [2]. These perturbations cause a rippled-shock wave which propagates in the target during the shell-compression phase [3]. When the rippled-shock wave breaks a flat rear surface of the target, a perturbation arises on the rear surface due to the nonuniformity of the shock wave [4]. This phenomenon is called "feed-in." After the shock breakout, a rarefaction wave propagates from the rear surface back to the laser-irradiated surface. Once the rarefaction wave reaches the laser-irradiated surface, the target starts to accelerate. When the rarefaction front is rippled, a perturbation arises on the laser-irradiated surface because the rarefaction arrives at a different time for the trough and the crest. This is called "feed-out" of the perturbation [5,6].

The feed-out is essential for the hydrodynamic instability analysis in ICF targets because the initial roughness on the rear surface of ICF targets is generally much greater than that on a laser-irradiated surface. There are a number of hydrodynamic instability experiments on the laser-irradiated surface (or x-ray irradiated surface). However, to date, the hydrodynamic phenomena related to the rarefaction wave have not been experimentally investigated in laser-irradiated targets, except for a few experimental studies in radiation drive targets [5]. Also, there is no direct measurement of the feed-out amplitude caused by rear surface perturbations.

In this Letter, we report the first experimental study on the feed-out effect in laser-irradiated target. Flat polystyrene (PS) targets were irradiated directly by partially coherent light [7]. Initial perturbations were imposed on the rear surface. We measured the perturbations both on the laser-irradiated surface and the rear surface with the side-on x-ray backlighting technique. We also measured the areal-density perturbation with the face-on x-ray backlighting technique. The spatial phase inversion of the perturbation on the rear surface was observed. We also observed the perturbation generated on a laser-irradiated surface due to a rippled rarefaction wave. Experimental results are well reproduced by a simple model with unperturbed hydrodynamic quantities calculated from a one-dimensional (1D) simulation.

A schematic view of the experimental setup is shown in Fig. 1. Initially perturbed PS (C_8H_8, $\rho = 1.056$ g/cm^3) foil targets were used for the experiments. The average thickness of the foils was 25 μm. Initial perturbations were imposed on the rear surface of the foils, whereas the laser-irradiated surface was flat. We imposed the initial perturbation by the thermal-press technique [8]. Perturbation wavelength and peak-to-valley amplitude were 100 and 10 μm, respectively. We used partially coherent light (PCL) [7] as the irradiation laser. The energy of the frequency doubled PCL ($\lambda = 0.53$ μm) provided by the Gekko XII glass laser system [9] was up to 300 J/beam. Two beams irradiated the PS foils with the incidence angle of 31.7° from the target normal for each beam. The spot diameter was approximately 600 μm. The pulse shape was flat-topped with FWHM of 2.3 ns. The rise time and the decay time were 50 and 150 ps, respectively. The intensity on the target was 6×10^{13} W/cm^2. We employed random phase plates [10] to further improve the uniformity. The time-integrated nonuniformity of the PCL on the target was 2.4% from the smooth envelope.

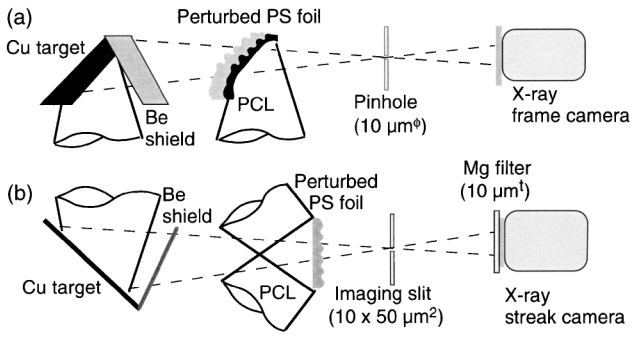

FIG. 1. Schematic view of the experimental setup. We measured the perturbation two ways: (a) side-on x-ray backlighting and (b) face-on x-ray backlighting.

We measured spatial perturbations by two ways: (a) side-on x-ray backlighting technique and (b) face-on x-ray backlighting technique. We employed the side-on x-ray backlighting technique to observe surface perturbations both on the laser-irradiated surface and the rear surface. A copper (Cu) foil with 20-μm thickness was used for backlighter targets. A beryllium (Be) foil of 10-μm thickness was placed between the backlighter and the PS target to avoid preheating of the PS target due to soft x-ray emission from the backlighter. A backlit image was obtained by two pinholes with 10-μm diameter onto a copper iodine (CuI) photocathode of an x-ray frame camera. A Be filter of 20-μm thickness was located in front of the photocathode to eliminate the self-emission from the PS target. In the side-on measurements, we limited the target width to 150–200 μm to avoid the bending of the target along the line of sight. Magnification of the pinhole imager was 30. Temporal resolution of the x-ray frame camera was 90 ps. The image data were recorded with a charge-coupled device camera. We obtained images for two timings in each laser shot with 0.5-ns intervals. We also employed the face-on x-ray backlighting technique to measure the areal-density perturbation of the irradiated foils. A Cu backlighter coupled with a Be filter was also used for the face-on measurement. A backlit face-on image was obtained by a slit (10-μm width $\times$ 50-μm height) with magnification of 28 onto a CuI photocathode of an x-ray streak camera. A magnesium filter of 10-μm thickness was placed in front of the photocathode of the x-ray streak camera to eliminate the high-energy component above its K-shell absorption edge ($\approx$1.31 keV). The resulting x-ray energy range was from 1.15 to 1.3 keV. Temporal resolution of the x-ray streak camera for the measurement was about 100 ps. The spatial resolution was measured using a backlit Fresnel zone plate [11]. The measured spatial resolution function, approximated as a sum of two Gaussian functions, is $R(u) = [1/(1 + \alpha)] \times \exp[-u^2/(2\sigma_1^2)] + \alpha \exp[-u^2/(2\sigma_2^2)]$, where $\alpha = 0.19$, $\sigma_1 = 5.63$ μm, and $\sigma_2 = 20.0$ μm.

We started by making a supplemental measurement to characterize the dynamics of the irradiated foil under our experimental condition. We measured the timings of shock breakout and rarefaction breakout by the side-on x-ray backlighting technique with the x-ray streak camera. A flat PS foil of 25-μm thickness was irradiated by the PCL, and we observed the motion of the foil from the side just like the measurement of the target trajectory in previous Rayleigh-Taylor experiments [12]. From the measurement, the shock wave breaks out at 0.73 $\pm$ 0.1 ns after the onset of the laser irradiation, and the laser-irradiated surface starts to accelerate at 1.19 $\pm$ 0.1 ns. From the shock breakout time, we calculated the shock velocity to be $(3.4 \pm 0.4) \times 10^6$ cm/s. We compared the experimental trajectories with a 1D hydrodynamic code ILESTA-1D [13]. From the 1D simulation, the shock front breaks out the rear surface at 0.75 ns. The rarefaction reaches the laser-irradiated surface at 1.12 ns. The comparison between the experiment and the simulation shows that there is little discrepancy with the shock and the rarefaction breakout time. This agreement justifies the use of the unperturbed hydrodynamic quantities calculated from the 1D simulation for the subsequent discussions.

Figures 2(a)–2(d) show the data by the side-on x-ray backlighting. We made two identical laser shots and obtained four snapshots in total. At 0.35 ns [Fig. 2(a)], the shock wave does not reach to the rear surface, that is, a plane shock wave is propagating in the PS foils. From the 1D simulation, the shock wave reaches the thinnest portion ($d = 20$ μm) of the target at about 0.6 ns and the thickest portion ($d = 30$ μm) at about 0.9 ns. Thus, at 0.85 ns [Fig. 2(b)], the shock wave is "passing" through the rear surface. We separately made spatial calibration between two frames of the x-ray framing camera. The lines in Fig. 2 show the same spatial position between the two images. The phase relationships indicate that the phase of rear surface perturbation inverts between 0.35 and 0.85 ns. Figures 2(c) and 2(d) are the images at later timings (0.88 and 1.38 ns). From the simulation, the rarefaction from the thinnest portion of the target reaches the laser-irradiated surface at 0.9 ns, whereas the rarefaction from the thickest portion reaches the laser-irradiated surface at 1.34 ns.

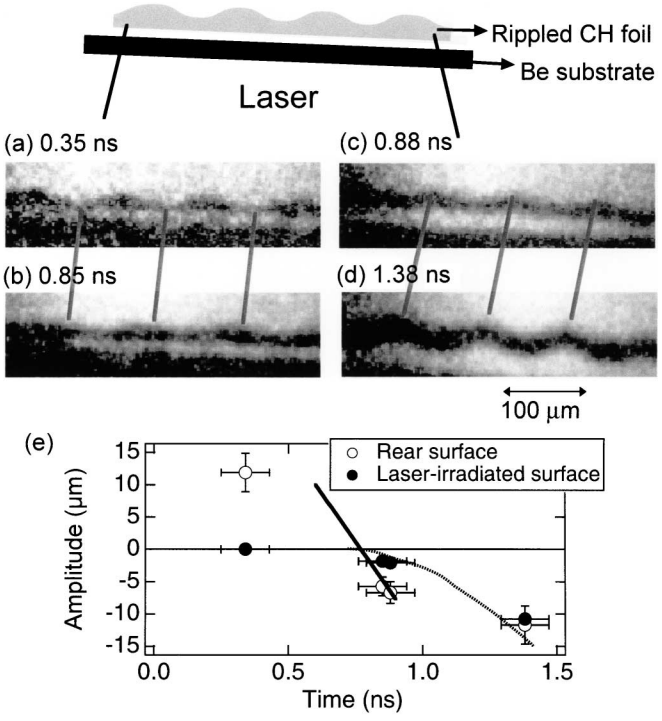

FIG. 2. Side-on backlit 2D image at (a) 0.35, (b) 0.85, (c) 0.88, and (d) 1.38 ns. Lines between the images indicate relationships of the phase. (e) Plot of the peak-to-valley amplitude of rear surface (open circles) and front surface (closed circles). Negative values mean phase inversion. The solid line is the calculated rear-surface amplitude by the simple model with 1D simulation. The dashed curve is the calculated amplitude of the laser-irradiated surface by the simple model.

The thinnest portion starts to move earlier than the thickest portion, thereby imposing the surface perturbation on the laser-irradiated surface. Figure 2(d) shows that perturbations arise on the laser-irradiated surface after the arrival of the rarefaction. The boundary between the high density target and the surrounding low density corona was depicted by tracing a position where the x-ray fluence becomes a mean value of the peak and valley. The mass density at the rear surface after the shock breakout is expected, from the target width of about 200 μm, to be less than 5% of the initial density. Thus the observed rear surface indicates the rarefaction tail.

Figure 2(e) shows the plot of perturbation amplitudes on the laser-irradiated surface and the rear surface. Negative values show that the phase of the perturbation is the reverse of the initial rear surface perturbation. We will compare the experimental results with a simple model based on a 1D simulation. Figure 3 shows the schematic picture of this model. Once the shock front reaches the thinnest portion of the target, the rear surface (rarefaction tail) moves faster than the shock velocity v_s because of the decompression. The velocity of the rear surface (v_r) is nearly constant to be 5.9×10^6 cm/s from the ILESTA 1D simulation. Therefore, the amplitude of the rear surface peak-to-valley perturbation amplitude a_r is

$$a_r(t) = a_0 - v_r \tau , \tag{1}$$

where a_0 is the initial peak-to-valley amplitude, and τ is the time started when the shock reaches at the thinnest part of the target. We neglect the lateral flow perpendicular to the shock propagation because the hydrodynamic scale length $v_s t$ is very short ($v_s t \sim 7$ μm, $t \sim 0.3$ ns: the time required for the shock to finish passing through the rear surface) compared to the perturbation wavelength (100 μm). The solid line in Fig. 2(e) shows the rear surface peak-to-valley amplitude calculated from the simple model. The line starts at 0.6 ns (shock breakout at the thinnest portion) and ends at 0.9 ns (shock breakout at the thickest portion). This simple model agrees well with the experimental results.

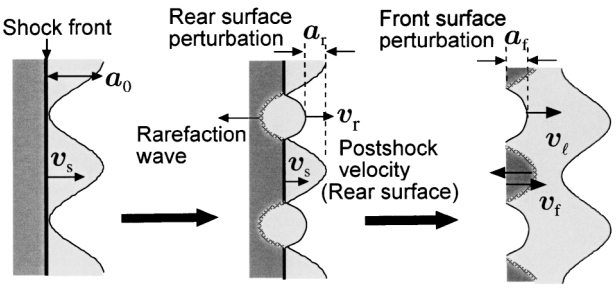

FIG. 3. A schematic view of the simple model. The amplitude of the rear surface and the laser-irradiated surface can be calculated from a couple of hydrodynamic parameters: the shock velocity v_s, the postshock velocity of the rear surface v_r, the constant velocity of the laser-irradiated surface v_f, and the velocity of the accelerated laser-irradiated surface v_ℓ.

Here we estimate the feed-out amplitude by another simple model with the 1D simulation. Before the rarefaction breakout, the laser-irradiated surface moves with a constant velocity v_f by the shock compression. The amplitude and phase of the rarefaction front do not change during its propagation. Once the rarefaction reaches the laser-irradiated surface, the surface accelerates and moves with a velocity $v_\ell(t)$. Thus the peak-to-valley amplitude on the laser-irradiated surface a_f is

$$a_f(t) = \int_{t_{rb}}^{t} [v_\ell(t') - v_f]\, dt', \tag{2}$$

where t_{rb} is the rarefaction breakout time at the thinnest portion. By using the values v_ℓ and v_f calculated from the 1D simulation, we draw $a_f(t)$ as a dotted curve in Fig. 2(e). We draw the curve from 0.9 ns (rarefaction breakout at the thinnest portion) to 1.34 ns (rarefaction breakout at the thickest portion). The experimental results are well reproduced by Eq. (2).

We also compare the experimental results with the analysis by Betti *et al.* [6]. They gave a formula of feed-out amplitude a_{fs} in Eq. (12) in their paper. From the experimental condition and the 1D simulation outputs, we obtained the parameters in the equation. Since the perturbation amplitude is relatively large in the experiment, the rarefaction breakout time t_{rb} in the equation is uncertain. If we take the rarefaction breakout time $t_{rb} \approx 0.9$ ns (rarefaction breakout at the thinnest portion), we obtain the feed-out amplitude a_{fs} to be $\approx$10.7 μm at 1.34 ns when the rarefaction completely reaches the laser-irradiated surface. If $t_{rb} \approx 1.34$ ns (rarefaction breakout at the thickest portion), we obtain $a_{fs} \approx 6$ μm. If we take the rarefaction breakout time $t_{rb} \approx 0.9$ ns (rarefaction breakout at the thinnest portion), we obtain the feed-out amplitude a_{fs} to be $\approx$10.7 μm at 1.34 ns when the rarefaction completely reaches the laser-irradiated surface. The calculated feed-out amplitude shows reasonable agreement with our experimental results ($a_f \approx 11$ μm at $t = 1.34$ ns).

We also measured the areal-density perturbation of the foil. We analyzed the temporal evolution of the areal-density perturbation by taking into account the spatial resolution of the diagnostics, the mass absorption coefficient of the PS foil, and the intensity distribution of the backlighter. Analyzed areal-density perturbation is shown in Fig. 4. Although the spatial phase on the rear surface perturbation inverts at 0.6–0.9 ns, the areal-density perturbation keeps its initial spatial phase during this phase inversion period. This is because the column mass integrated from the rarefaction front to the tail is nearly conserved. After the rarefaction wave completely reaches the laser-irradiated surface ($\geq$1.3 ns), the fundamental mode amplitude begins to increase due to the Rayleigh-Taylor instability growth. The second harmonic component arises with a "negative" phase of the initial fundamental mode of the areal-density perturbation after 0.9 ns at which the rarefaction first arrives on the laser-irradiated surface. The

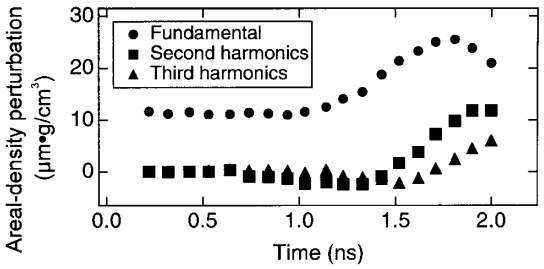

FIG. 4. Temporal evolution of the areal-density perturbation for fundamental mode (circles), second harmonic component (squares), and third harmonic component (triangles). Negative values mean that the phase of the components are inverted.

third harmonic component rises slightly at 1 ns. The higher harmonics turn into "positive" phase in later time because of nonlinear saturation of the RT growth. Similar results have been observed in previous experimental works in the x-ray drive experiments [5], but the origin of the higher harmonics before the rarefaction breakout was not given. We consider that the growth of the rear surface perturbation causes the higher harmonics because of the coupling of a vortex and the Richtmyer-Meshkov instability [14]. When the shock wave passes through the curved surface, a vortex arises and shifts the contact surface due to the lateral mass flow, resulting in the higher harmonic generation. Another possible candidate for the negative higher harmonic generation is the lateral mass flow during the rarefaction breakout at the laser-irradiated surface. When the crest of the rarefaction front reaches the laser-irradiated surface, a dent is generated followed by lateral mass flow (Fig. 3, right). This dent causes negative harmonics in the column-density perturbation.

In conclusion, we have experimentally investigated the feed-out effect in the start-up phase of ICF targets. The laser-irradiated surface is perturbed by the rippled rarefaction wave generated at the perturbed rear surface. Our experimental results are in agreement with both the very simple model and the analytic model by Betti *et al.* These experimental results would give an important index for the design of ICF targets.

The authors gratefully acknowledge the technical staffs of the Institute of Laser Engineering, Osaka University. This work is partly supported by the Japan Society for Promotion of Science (JSPS).

*Present address: National Institute for Fusion Science, Toki, Gifu, 509-5202 Japan.

[1] S. Chandrasekhar, *Hydrodynamic and Hydromagnetic Stability* (Oxford University Press, London, 1968), Chap. 10.
[2] H. Azechi *et al.*, Phys. Plasmas **4**, 4079 (1997); R. J. Taylor *et al.*, Phys. Rev. Lett. **76**, 1643 (1996); D. H. Kalantar *et al.*, Phys. Rev. Lett. **76**, 3574 (1996); E. Wolfrum *et al.*, Phys. Plasmas **5**, 227 (1998); C. J. Pawley *et al.*, Phys. Plasmas **4**, 1969 (1997); V. A. Smalyuk *et al.*, Phys. Plasmas **6**, 4022 (1999).
[3] T. Endo *et al.*, Phys. Rev. Lett. **74**, 3608 (1995).
[4] R. Ishizaki *et al.*, Phys. Rev. E **53**, 5592 (1996); K. Nishihara and R. Ishizaki, Phys. Plasmas **5**, 1945 (1998).
[5] D. P. Smitherman *et al.*, Phys. Plasmas **6**, 932 (1998); **6**, 940 (1998).
[6] R. Betti *et al.*, Phys. Rev. Lett. **81**, 5560 (1998).
[7] H. Nakano *et al.*, Appl. Phys. Lett. **63**, 580 (1993); K. Mima *et al.*, Phys. Plasmas **3**, 2077 (1996).
[8] K. Shigemori *et al.*, *Annual Progress Report of Institute of Laser Engineering* (Osaka University Press, Osaka, 1995), p. 135.
[9] C. Yamanaka *et al.*, Nucl. Fusion **27**, 19 (1987).
[10] Y. Kato *et al.*, Phys. Rev. Lett. **53**, 1057 (1984).
[11] M. Matsuoka *et al.*, Rev. Sci. Instrum. **70**, 637 (1999).
[12] K. Shigemori *et al.*, Phys. Rev. Lett. **78**, 250 (1997).
[13] H. Takabe *et al.*, Phys. Fluids **31**, 2884 (1988).
[14] J. G. Wouchuk and K. Nishihara, Phys. Plasmas **3**, 3761 (1996); **4**, 1028 (1997).